

1 **On-line Optimization of Four-Zone Simulated Moving Bed**
2 **Chromatography using an Equilibrium-Dispersion Model:**

3 **II. Experimental Validation**

4
5 Ju Weon Lee^{1,*}, Achim Kienle^{1,2}, and Andreas Seidel-Morgenstern^{1,3}

6
7 ¹ Max-Planck-Institute for Dynamics of Complex Technical Systems
8 Sandtorstr. 1, 39106 Magdeburg, Germany

9 ² Institute of Automation Technology, Otto von Guericke University
10 Universitätsplatz 2, 39106 Magdeburg, Germany

11 ³ Institute of Process Engineering, Otto von Guericke University
12 Universitätsplatz 2, 39106 Magdeburg, Germany

13
14
15 *: Corresponding Author

16 Tel: +49 391 6110392

17 Fax: +49 391 6110521

18 Email: lee@mpi-magdeburg.mpg.de

1 **Abstract**

2 In the first theoretical part of this work, an on-line optimization method using the equilibrium-
3 dispersion model of chromatography was developed and successfully demonstrated for the dynamic
4 optimization of periodically operated four-zone simulated moving bed (SMB) processes. In this
5 second part, we present the experimental validation of the proposed concept. To describe the behaviors
6 of real SMB systems, the on-line control unit was modified. Unavoidable system void volumes, which
7 can be described using delay functions corresponding to standard mass balance models for pipes and
8 CSTs, were considered in addition to the chromatographic columns. Furthermore, new sample
9 collection method that does not interrupt product streams was introduced for process monitoring. The
10 equipment including an external concentration analysis unit was automated via a tailor-made interface
11 program. The on-line control unit estimated the parameters of the process model and optimized the
12 future operating conditions 'switch-by-switch'. The case study investigated in this work was the
13 separation of racemic mixtures of two bicalutamide enantiomers using a chiral stationary phase
14 applying the conventional and two advanced SMB operating modes.

15

16 **Keywords:** On-line optimization, Simulated moving bed chromatography, Equilibrium-dispersion
17 model, Mixing cell with active counteraction scheme, Experimental validation, Bicalutamide
18 enantiomers

19

20

1. Introduction

Simulated moving bed (SMB) process has been widely applied for the separations of difficult mixtures since it was introduced in 1960s [1]. Because of the periodic operation characteristics, the SMB process does not reach a steady-state but only a cyclic steady-state (CSS). This means that the process outputs at a certain time of the cycle does not represent the state of the process. Identification of the average process outputs in one or multiple port switching intervals requires a complex sample collection and an extra analysis apparatus. Because of this process monitoring difficulty, SMB process control and optimization research was mostly focused on the theoretical approaches [2-6]. Only few experimental validations were presented connected with highly expensive process monitoring units, such as the fixed port observation for the internal concentration profiles [7, 8], the ‘cycle to cycle’ observation of the average product stream concentrations [9], and the foot-print observation, which is the periodical patterns of the elution bands, using the on-line detectors in the product streams [10].

In the first part of this work [11], we developed an on-line optimization technique that uses model based prediction with the equilibrium-dispersion model. We applied the concept to analyze the four-zone SMB process that has no system void volume and exploits columns with identical properties. Owing to the availability of the mixing cell with active counteraction (MC-AC) scheme that can provides accurate and rapid numerical solutions of the process model [12], the control unit can quickly estimate the model parameters and identify optimized operating conditions. However, practical application of this concept still requires further improvement to evaluate unavoidable system void volumes and monitoring strategies for dynamic optimization of a real SMB process.

The conventional four-zone SMB process consists of at least four chromatographic columns (one column per zone) and more devices, such as pumps, valves, detectors, and fittings to connect all elements properly. In pilot-scale SMB chromatography, the volume of these additional devices, also known as the system void volumes, are relatively small compared to the column volumes, so that they were often ignored or handled as a part of the column volume [13] or port switching interval compensation [14]. However, this simplification causes problems for high purity separation due to unexpected and unwanted remixing and retention of mixture components. To avoid these problems,

1 various designs were introduced to reduce the system void volumes and trace the system void volumes
2 by switching the ports asynchronously [15, 16]. Moreover, various advanced operational concepts and
3 structural configurations, such as intermittent flow variation and asynchronous port switching were
4 introduced to enhance process performance [17].

5 In this work, two types of system void volume models – a pipe model without dispersion
6 (zeroth-order delay) and an ideal mixer model (first-order delay) – were implemented in the process
7 model, which is based on the equilibrium-dispersion column model, to estimate the process states in
8 the columns and various structures of the system void volumes. Since this extended process model can
9 estimate hold-up and remixing of components that take place inside of the system void volumes, a new
10 sample collection method can be applied, which does not interrupt the continuity of the product
11 streams. A pilot-scale SMB system was used for the experimental validation of the proposed on-line
12 optimization concept considering the separation of two bicalutamide enantiomers. For the
13 experimental validation of the concepts introduced in the first part of this work, the same two
14 advanced SMB operating modes, namely the outlet stream swing (OSS) [18] and the flow-focusing
15 (FF) [11, 19] operating modes were applied.

16

17 **2. Process Model and Optimization Strategy**

18 The basic process model (the equilibrium-dispersion column model with its numerical solver
19 and the boundary conditions determined by the operating modes) and dynamic optimization strategies
20 (the objective function for parameter estimation and the cost function for future prediction) were
21 described in detail in the first part of this work [11].

22 Figure 1 shows the design steps with the on-line optimization and the schematic flow-diagram
23 of the online optimization proposed in the first part of this work. The on-line optimization technique
24 can be applied to the pilot-scale research with the minimum information acquired from the preliminary
25 and small scale design steps. In this proposed design concept, it is not required to measure the model
26 parameters in time-consuming preliminary experiments. Thus, the following process simulation step

1 can be omitted, which is often performed in the conventional design (Figure 1 in [11]) with the model
 2 parameters. Since the proposed control unit exploits the information of the rigorous chromatographic
 3 process model (the equilibrium-dispersion model), parameter estimation and process optimization are
 4 done during the process validation in the pilot-scale research step.

5 A real SMB process is set up using several packed chromatographic columns, pipes, and
 6 fittings with a ring connection. Therefore, not only the mass balances for the columns but also the
 7 mass balances for the system void volumes should be considered in the process model. In the
 8 following sections (Sections 2.1 and 2.3), we will briefly describe the column models and the
 9 optimization strategies. Newly considered additional system void volume models and new process
 10 monitoring strategies considered and implemented in this work will be described in Sections 2.2 and
 11 2.4, respectively.

12

13 ***2.1. Column model and SMB operating modes***

14 For the simulation of the concentration profiles in the column, the equilibrium-dispersion
 15 model with bi-Langmuir adsorption isotherms was used as,

$$16 \quad v_L \frac{\partial c_i}{\partial z} + \varepsilon \frac{\partial c_i}{\partial t} + (1 - \varepsilon) \frac{\partial q_i}{\partial t} = D_{a,i} \frac{\partial^2 c_i}{\partial z^2} \quad \forall i \in \mathbf{N}_S \quad (1)$$

$$17 \quad q_i = q_{1,Max} \frac{K_1 c_i}{1 + K_1 \sum_{l \in \mathbf{N}_S} c_l} + q_{2,Max} \frac{K_{2,i} c_i}{1 + \sum_{l \in \mathbf{N}_S} K_{2,l} c_l} \quad (2)$$

18 where v_L is the linear velocity of the liquid phase, ε is the column void fraction, D_a is the apparent
 19 dispersion coefficient, $q_{1,Max}$ and $q_{2,Max}$ are respectively the maximum adsorption capacity of the
 20 achiral and chiral active sites of the stationary phase, K is the equilibrium constant, and \mathbf{N}_S is the
 21 solute set.

22 The boundary conditions of each zone inlet can be determined from the operating conditions.
 23 Three operating modes, the standard (Std), the outlet stream swing (OSS), and the flow focusing (FF)
 24 operating modes were applied. They were implemented as described below,

- 1 • Standard (Std) operating mode

2
$$Q_{L,Z1}^{Std} = Q_{L,Z4}^{Std} + Q_{L,Dsrb}^{Std}, \quad c_{i,Z1In}^{Std} = \frac{c_{i,Z4Out}^{Std} Q_{L,Z4}^{Std} + c_{i,Dsrb}^{Std} Q_{L,Dsrb}^{Std}}{Q_{L,Z4}^{Std} + Q_{L,Dsrb}^{Std}} \quad (3)$$

3
$$Q_{L,Z2}^{Std} = Q_{L,Z1}^{Std} - Q_{L,Extr}^{Std}, \quad c_{i,Z2In}^{Std} = c_{i,Extr}^{Std} = c_{i,Z1Out}^{Std} \quad (4)$$

4
$$Q_{L,Z3}^{Std} = Q_{L,Z2}^{Std} + Q_{L,Feed}^{Std}, \quad c_{i,Z3In}^{Std} = \frac{c_{i,Z2Out}^{Std} Q_{L,Z2}^{Std} + c_{i,Feed}^{Std} Q_{L,Feed}^{Std}}{Q_{L,Z2}^{Std} + Q_{L,Feed}^{Std}} \quad (5)$$

5
$$Q_{L,Z4}^{Std} = Q_{L,Z3}^{Std} - Q_{L,Raff}^{Std}, \quad c_{i,Z4In}^{Std} = c_{i,Raff}^{Std} = c_{i,Z1Out}^{Std} \quad (6)$$

- 6 • Outlet stream swing (OSS) operating mode [18]

7 Step 1: Extract stream off

8
$$Q_{L,Z1}^{OSS1} = Q_{L,Z2}^{OSS1} = Q_{L,Z1}^{Std} \quad (7)$$

9
$$Q_{L,Z3}^{OSS1} = Q_{L,Z1}^{Std} + Q_{L,Feed}^{Std} \quad (8)$$

10
$$Q_{L,Z4}^{OSS1} = Q_{L,Z1}^{Std} + Q_{L,Feed}^{Std} - Q_{L,Extr}^{Std} - Q_{L,Raff}^{Std} \quad (9)$$

11
$$t_S^{OSS1} = \frac{Q_{L,Raff}^{Std}}{Q_{L,Extr}^{Std} + Q_{L,Raff}^{Std}} (1 - F_{Op}^{OSS}) t_S^{Std}, \quad 0 \leq F_{Op}^{OSS} \leq 1 \quad (10)$$

12 Step 2: Standard operation

13
$$Q_{L,j}^{OSS2} = Q_{L,j}^{Std}, \quad \forall j \in \{Z1, \dots, Z4\} \quad (11)$$

14
$$t_S^{OSS2} = F_{Op}^{OSS} t_S^{Std} \quad (12)$$

15 Step 3: Raffinate stream off

16
$$Q_{L,Z1}^{OSS3} = Q_{L,Z1}^{Std} \quad (13)$$

17
$$Q_{L,Z2}^{OSS3} = \max(0, Q_{L,Z1}^{Std} - Q_{L,Extr}^{Std} - Q_{L,Raff}^{Std}) \quad (14)$$

18
$$Q_{L,Z3}^{OSS3} = Q_{L,Z4}^{OSS3} = Q_{L,Z1}^{Std} - Q_{L,Extr}^{Std} - Q_{L,Raff}^{Std} + Q_{L,Feed}^{Std} \quad (15)$$

19
$$t_S^{OSS3} = \frac{Q_{L,Extr}^{Std}}{Q_{L,Extr}^{Std} + Q_{L,Raff}^{Std}} (1 - F_{Op}^{OSS}) t_S^{Std} \quad (16)$$

- 20 • Flow focusing (FF) operating mode [11, 19]

21 Step 1: Internal circulation

22
$$Q_{L,Z1}^{FF1} = Q_{L,Z2}^{FF1} = Q_{L,Z3}^{FF1} = Q_{L,Z4}^{FF1} = Q_{L,Z4}^{Std} \quad (17)$$

23
$$t_S^{FF1} = F_{Pos}^{FF} (1 - F_{Op}^{FF}) t_S^{Std}, \quad 0 \leq F_{Pos}^{FF} \leq 1, \quad 0 < F_{Op}^{FF} \leq 1 \quad (18)$$

24 Step 2: Focused external flows

$$1 \quad Q_{L,Z1}^{FF2} = Q_{L,Z4}^{Std} + Q_{Feed}^{Std}/F_{Op}^{FF} \quad (19)$$

$$2 \quad Q_{L,Z2}^{FF2} = Q_{L,Z4}^{Std} + (Q_{L,Feed}^{Std} - Q_{L,Extr}^{Std})/F_{Op}^{FF} \quad (20)$$

$$3 \quad Q_{L,Z3}^{FF2} = Q_{L,Z4}^{Std} + (Q_{L,Feed}^{Std} - Q_{L,Extr}^{Std} + Q_{L,Feed}^{Std})/F_{Op}^{FF} \quad (21)$$

$$4 \quad Q_{L,Z3}^{FF2} = Q_{L,Z4}^{Std} + (Q_{L,Feed}^{Std} - Q_{L,Extr}^{Std} + Q_{L,Feed}^{Std} - Q_{L,Raff}^{Std})/F_{Op}^{FF} \quad (22)$$

$$5 \quad t_s^{FF2} = F_{Op}^{FF} t_s^{Std} \quad (23)$$

6 Step 3: Internal circulation

$$7 \quad Q_{L,Z1}^{FF1} = Q_{L,Z2}^{FF1} = Q_{L,Z3}^{FF1} = Q_{L,Z4}^{FF1} = Q_{L,Z4}^{Std} \quad (24)$$

$$8 \quad t_s^{FF3} = (1 - F_{Pos}^{FF})(1 - F_{Op}^{FF})t_s^{Std} \quad (25)$$

9 where Q_L is the volumetric flow-rate of the mobile phase, the subscripts, *Dsrb*, *Extr*, *Feed*, and *Raff*
10 respectively denote the desorbent, extract, feed, and raffinate (cf. Figure 2a), t_s is the port switching
11 interval, F_{Op} is the operation factor, F_{Pos}^{FF} is the position factor of the focused flows, and the subscripts,
12 Zn , $ZnIn$, and $ZnOut$ denote the n^{th} zone and its inlet and outlet, respectively. If the operation factors
13 of the OSS and FF operating modes are equal to 1, the advanced operating modes reduce to the
14 standard operating mode.

15

16 **2.2. System void volume models**

17 Since the columns are connected with the above-mentioned additional devices, unavoidable
18 system void volumes in SMB units need to be considered. To describe the retention and remixing of
19 mixture components in the system void volumes, the size and structure of the system void volumes
20 need to be analyzed. Figure 2a shows the schematic flow-diagram of the SMB unit including the
21 system void volumes. In the column switching region of the SMB ring (inside of the dotted circle), the
22 pipes connected with the inlets and outlets of the columns (gray arrows) can be considered as a part of
23 the connected column by increasing the void fractions of the column or adjusting the adsorption
24 isotherm parameters. However, the void volumes located outside of the SMB ring can cause
25 significant latency and deformation of the concentration profiles in the feed and product streams,
26 which results in delayed process input and output information. Some void volumes in the SMB ring do

1 not switch the positions following a column position switching (cf. the void volumes inside of the
 2 orange colored region in Figure 2), so that these void volumes cause remixing of the internal
 3 concentration profiles. Since both are critical in aspects of SMB process optimization for high purity
 4 separation, two void volume assumptions were used to evaluate all system void volumes; one is
 5 considering a void volume as a delay lag (Lag; zeroth-order delay), and the other assumes an ideal
 6 mixer (Mixer; first-order delay).

7 In the first theoretical part of this work, the column mass balance was basically solved with the
 8 mixing cell (MC) model, which is equivalent to the first-order finite volume method and the basis of
 9 the MC-AC scheme, so that the flows are also discretized to the volume segment,

$$10 \quad \bar{c}_{i,j}^n = \frac{1}{v_n} \int_{v_n^0}^{v_n^0+v_n} c_{i,j}(v) dv \quad (26)$$

11 where $\bar{c}_{i,j}^n$ is the average concentration of solute i in the n^{th} volume segment of the flow j , v_n^0 is the
 12 volumetric position of the front end of the n^{th} volume segment, and v_n is the volume of the n^{th} volume
 13 segment.

14 Assuming that there is no mixing in a Lag void volume, i.e. a plug-flow occurs in a pipe, the
 15 shape of the input concentration profile is conserved at the output with a certain volume latency. This
 16 corresponds to a first-in-first-out (FIFO) queue data structure. Depending on the size of the Lag void
 17 volume, the outlet concentration was calculated as,

$$18 \quad \bar{c}_{i,LagIn}^n = \bar{c}_{i,Lag}^1 \quad (27)$$

$$19 \quad \bar{c}_{i,Lag}^m(v|v_m^0 \leq v \leq v_m^0 + v_m) = \bar{c}_{i,Lag}^{m+1}(v|v_m^0 + v_n \leq v \leq v_m^0 + v_m + v_n) \quad (28)$$

$$20 \quad \bar{c}_{i,LagOut}^n = \frac{1}{v_n} \int_{V_{Lag}}^{V_{Lag}+v_n} c_{i,Lag}(v) dv \quad (29)$$

21 where V_{Lag} is the volume of the Lag, v_m is the volume of the m^{th} volume segment captured in the Lag,
 22 and the subscripts, *LagIn* and *LagOut* denote the inlet and outlet flows of the Lag void volume,
 23 respectively. The volume segment newly entering the Lag void volume ($\bar{c}_{i,LagIn}^n$) is stacked at the inlet
 24 of the void volume, cf. Eq. (27). All volume segments previously stacked are shifted as according to
 25 the size of new volume segment, cf. Eq. (28). Then the extra volume at the outlet of the Lag is cut to
 26 the outlet volume segment with averaged concentration, cf. Eq. (29). Thus, the size of the Lag void

1 volume is maintained and the concentration profiles that migrate through the Lag void volume are
 2 latent as the size of the Lag void volume.

3 In contrast, in Mixer void volumes, the input volume segment is completely mixed with the
 4 solution held in the Mixer, while an identical volume leaves.

$$5 \quad \bar{c}_{i,Mixer}^* = \bar{c}_{i,MixerIn}^n + (\bar{c}_{i,Mixer} - \bar{c}_{i,MixerIn}^n) \exp\left(-\frac{v_n}{V_{Mixer}}\right) \quad (30)$$

$$6 \quad \bar{c}_{i,MixerOut}^n = \bar{c}_{i,MixerIn}^n - \left(\frac{V_{Mixer}}{v_n}\right) (\bar{c}_{i,Mixer} - \bar{c}_{i,MixerIn}^n) \left\{ \exp\left(-\frac{v_n}{V_{Mixer}}\right) - 1 \right\} \quad (31)$$

7 where V_{Mixer} is the volume of the Mixer, $\bar{c}_{i,Mixer}^*$ is the updated concentration of solute i in the Mixer
 8 after n^{th} volume segment enters, and the subscripts, $MixerIn$ and $MixerOut$ denote the inlet and
 9 outlet flows of the Mixer void volume, respectively.

10 Figure 2b shows the structure of the system void volumes in combination with columns
 11 considered in this work. The feed mixture flows through the feed stream and mixed with the zone 2
 12 outlet stream at the outside of the SMB ring and the mixed stream enters again to the zone 3 in the
 13 SMB ring, so that one Lag and one Mixer void volume models were applied for the feed stream. At
 14 the raffinate and extract ports, the streams flow to the opposite direction of the feed stream. Additional
 15 CSTs were connected at the ends of the product streams to observe the process outputs. A detailed
 16 sample collection strategy is described in the following section 2.4. A solute-free solvent was used as a
 17 desorbent and the system was filled with solute-free solvent at the beginning, so that there is no Lag
 18 void volume in the desorbent stream, but a relatively large volume of CST, which mix desorbent and
 19 the zone 4 outlet effluent, was used to collect samples at the recycle stream.

20

21 **2.3. Parameter estimation and optimization of operating conditions**

22 The control unit estimated the isotherm parameters and dispersion coefficients with the same
 23 objective function, G to be minimized as used in the first part of this work [11],

$$24 \quad G(D_{L,i}, q_{1,Max}, K_1, q_{2,Max}, K_{2,i}) = \sum_{\forall i \in \mathbf{N}_S, \forall j \in \mathbf{N}_O, \forall k \in \mathbf{H}_P} \left(\left(C_{i,j,k}^{Exp} \right)^{w_P} \frac{|c_{i,j,k}^{Cal} - c_{i,j,k}^{Exp}|}{C_{i,j,k}^{Exp}} \right) \quad (32)$$

25 where w_P is the power of weight factors, \mathbf{N}_O is the observed port set, \mathbf{H}_P is the control cycle set in the

1 receding past horizon, the superscripts, *Cal* and *Exp* denote the values calculated by the control unit
 2 and obtained from the process, respectively.

3 Also the same cost functions were used as in the first part of this work to decide the optimized
 4 future operations,

$$5 \quad H = \sum_{j \in \{Z1, \dots, Z4\}} H_j \quad (33)$$

$$6 \quad H_{Z1} = \left(\frac{c_{(R),Rcyl,P_F}^{Cal} - C_{(R),Rcyl}}{C_{(R),Rcyl,P_F}} \right)^2, \quad C_{(R),Rcyl} = \hat{R}_{(R),Rcyl} C_{(R),Raff} \quad (34)$$

$$7 \quad H_{Z2} = \left(\frac{c_{(S),Extr,P_F}^{Cal} - C_{(S),Extr}}{C_{(S),Extr}} \right)^2, \quad C_{(S),Extr} = \frac{(1 - \hat{P}u_{Extr})}{\hat{P}u_{Extr}} \left(\sum_{i \in N_S} c_{i,Extr,P_F}^{Cal} - c_{(S),Extr,P_F}^{Cal} \right) \quad (35)$$

$$8 \quad H_{Z3} = \left(\frac{c_{(R),Raff,P_F}^{Cal} - C_{(R),Raff}}{C_{(R),Raff}} \right)^2, \quad C_{(R),Raff} = \frac{(1 - \hat{P}u_{Raff})}{\hat{P}u_{Raff}} \left(\sum_{i \in N_S} c_{i,Raff,P_F}^{Cal} - c_{(R),Raff,P_F}^{Cal} \right) \quad (36)$$

$$9 \quad H_{Z4} = \left(\frac{c_{(S),Rcyl,P_F}^{Cal} - C_{(S),Rcyl}}{C_{(S),Rcyl}} \right)^2, \quad C_{(S),Rcyl} = \hat{R}_{(S),Rcyl} C_{(S),Extr} \quad (37)$$

10 where H is the cost function, C is the desired set-value of future process output, \hat{R} is the designated
 11 concentration ratio of recycle stream to product stream impurities, $\hat{P}u$ is the designated product purity,
 12 the subscripts (R) and (S) respectively denote the more-retained component, (R) -bicalutamide and the
 13 less-retained component, (S) -bicalutamide, and the subscript P_F denotes the last control cycle of the
 14 future horizon. Note that the control cycle corresponds to one port switching interval as considered in
 15 the first part of this work.

16

17 **2.4. Sample collection strategy**

18 To collect information regarding the process outputs, small amount of samples were collected
 19 from the CSTs (Red CSTs in Figure 2a) at a defined time offset from the beginning of the port
 20 switching interval, cf. Figure 5. The lower graph in Figure 3a shows the schematic saw-tooth
 21 concentration histories of the extract stream. A narrow and low level impurity concentration profile
 22 (blue profile) forms at the beginning of the port switching interval. If the volume of the sampling CST
 23 is too small (the middle graph in Figure 3a), impurity is not retained in the sampling CST and a sample

1 collected with a wrong time offset (A in Figure 3a) cannot contain any impurity. As shown in the
2 lower and middle graphs of Figure 3a, the impurity component profile completely passes through the
3 small sampling CST before collecting the samples. Therefore, to avoid this problem the volume of the
4 sampling CST should be large enough to retain impurities in every cycle until the sample is collected
5 (upper graph in Figure 3a). In this work, the volume of the sampling CSTs in the product streams were
6 set to 40 ml to keep the volume approx. 2 – 8 times larger than the elution volumes of the product
7 streams.

8 Besides the desired separation effect of the column, the process outputs can be negatively
9 affected by the volume and structure of the system void volumes, so that precise simulation of the
10 system void volume behaviors as described in Section 2.2 is required. Since the purities obtained from
11 the process outputs does not represent the product purities, i.e. the process outputs are not average
12 concentrations in one control cycle, the control unit should take the estimated average concentrations
13 at the product ports or in the product effluents after the sampling CSTs. If the control unit takes the
14 purities at latter position in ‘Full sampling’ method (Figure 3b), the control unit may finds extreme
15 operating conditions due to the long residence time of impurities in the sampling CSTs. For example,
16 the control unit will find the operating conditions that result fast flow of product stream to wash out
17 the sampling CST if the sampling CST is highly contaminated. This kind of extreme operation can be
18 minimized applying a ‘By-pass sampling’ method as shown in Figure 3b. The ‘Full sampling’ method
19 was applied in this work, so that the product purities, the controlled variables were obtained from the
20 estimated average concentrations at the product ports.

21 To quantify the process performances, two essential performance factors of the overall
22 process, productivity and desorbent consumption (DC) were calculated as below,

$$23 \text{ Productivity} = \frac{\{\text{mass of (R)-bicalutamide in the extract stream for one control cycle}\}}{\{\text{Volume of adsorbent}\}\{\text{time of one control cycle}\}} \quad (38)$$

$$24 \text{ DC} = \frac{\{\text{Volume of solvent used for one control cycle}\}}{\{\text{mass of (R)-bicalutamide in the extract stream for one control cycle}\}} \quad (39)$$

25

26 **3. Experiments**

1
2
3
4
5
6
7
8
9
10
11
12
13
14
15
16
17
18
19
20
21
22
23
24
25
26

3.1. SMB Unit and Analytical HPLC for Online Monitoring

The SMB unit consists of one 48-port valve tower (C912, Knauer GmbH, Germany), four pumps (K-1800, Knauer GmbH, Germany), and two UV detectors (K-2501, Knauer GmbH, Germany). An HTS/PAL autosampler (CTC analytics AG, Swiss) collects samples from three sampling CSTs and injects them to an HPLC unit that consists of one pump (Smartline Pump 1000, Knauer GmbH, Germany), one UV detector (Smartline UV 2500, Knauer GmbH, Germany), and one column thermostat (Jetstream 2 Plus, Knauer GmbH, Germany). Four preparative columns (DAC column 2.5 cm I.D., Merck GmbH, Germany) packed with ChiralPak IA (20 μ m, Daicel Chemical Industries Ltd., Japan) were connected in the SMB unit with one column per zone configuration. An analytical column (ChiralPak IA, 3 μ m, 0.46 \times 15 cm, Daicel Chemical Industries Ltd., Japan) was used to analyze the collected samples.

In the analytical HPLC unit, HPLC grade methanol (VWR GmbH, Germany) was used as the mobile phase at 2.0 ml/min, the injection volume was 5.0 μ l, and the column temperature was fixed to 40 $^{\circ}$ C to analyze three samples in one port switching interval, 3 min. The wavelength of a UV detector was fixed to 300 nm.

3.2. Materials and procedures

In the SMB unit, ACS grade methanol (Merck GmbH, Germany) was used as the mobile phase. The feed mixture, racemic bicalutamide provided from AstraZeneca (Sweden) was dissolved in the same grade of methanol. The wavelength of both extract and raffinate port UV detectors were fixed to 300 nm. Four SMB columns were packed by dynamic axial compression method. 45 g of adsorbent was loaded in each column. The column properties were measured at room temperature. The mobile phase flow rate was 3.0 ml/min. 1,3,5-tri-tert-butylbenzene (TCI Europe nv, Belgium) was used as a tracer for void volume measurement. The properties of each column and average properties were listed in **Table 1**. The solubility of feed mixture at room temperature was 16.5 g/L. The feed concentrations were 14.1 g/L (7.0 g/L of (R)-bicalutamide and 7.1 g.L of (S)-bicalutamide) for the

1 fresh feed mixture and 12.8 g/L (5.9 g/L of (R)-bicalutamide and 6.9 g.L of (S)-bicalutamide) for the
2 recovered feed mixture from experiments with the fresh feed mixture. During the SMB experiments,
3 239 g of bicalutamide racemates was consumed. To recover feed mixture from collected effluent, a
4 rotary evaporator (R-220 Pro, Büchi GmbH, Germany) was used. The system void volumes were
5 measured as shown in **Figure 2b**. At the end of SMB experiment, the SMB ring was disconnected
6 between the zone 4 and desorbent port, and the desorbent flowed through the zone 1 to the zone 4 with
7 50 ml/min. At the outlet of the zone 4, a UV detector was connected to monitor the elution of
8 developed internal concentration profiles.

10 ***3.3. Communication between the on-line control unit and the SMB unit***

11 The control unit takes the concentrations collected in the sampling CSTs at a certain moment
12 as process outputs and provides four zone flow-rates as process inputs. Therefore, an SMB process
13 interface was applied, which can automate the process operation including an external analysis unit
14 and interpret raw process signals (Figure 4). All operation of the SMB process was automated via
15 serial communication (RS-232) with the tailored interface program developed with LabVIEW
16 (National Instruments Inc. Ver. 2011).

17 Three samples were consecutively collected at the extract, raffinate, and recycle sampling
18 CSTs at the preset time offsets from the beginning of every the control cycles, and directly injected to
19 the analytical HPLC system. This means that the HPLC chromatogram peaks that correspond to the
20 components of the monitored streams can be detected at the same elapsed time from the beginning of
21 the corresponding control cycle. Therefore, all components in three samples could be detected at the
22 different elution time, and the concentrations were quantitatively calibrated by the fixed interval
23 integration corresponding to the elution times of each component.

25 **4. Results**

1
2
3
4
5
6
7
8
9
10
11
12
13
14
15
16
17
18
19
20
21
22
23
24
25
26

4.1. Characteristics of columns

As shown in Table 1, all columns were well packed with the same length (0.38% of RSD). Based on the first part of this work, the number of cells per column was set to 25. The Henry's constants and the numbers of theoretical plates (NPTs) deviated quite significantly (~5% and ~35% of RSD, respectively). This means that the number of past process outputs should be a multiple of the number of columns to get uniform deviations of the process outputs in every control cycle. Because of the Lag void volume in the feed stream, the feed mixture was fed into the SMB system with a certain delay. This means that the process outputs at the first few cycles may contain less or no information (less or no elution of products). Therefore, the control unit started the parameter estimation from the 6th cycle (one cycle delay + four cycle process outputs + meaningless first cycle), and took at most 8 past process outputs were used for the parameter estimation. Same as the first part of this work, the number of future horizon to optimize future operating conditions was 6.

4.2. On-line control unit parameters

Figure 5 shows one representative chromatogram of the analytical HPLC unit. Three samples taken from the extract, recycle, and raffinate sampling CSTs were sequentially injected. It took 70 seconds to analyze one sample, and the peaks were eluted in the last 30 seconds. Therefore, the samples were injected every 40 seconds interval. Due to extra time for sample preparation (valve switching, syringe operation, ...) the offsets for the extract, recycle, and raffinate sample collections, $\{\text{Sample Collect Time}\}/\{\text{Cycle Time}\}$ were 0.067, 0.289, and 0.511, respectively.

If the control unit takes only the average concentrations, entire effluent of product stream should be collected and well-mixed before the sample collection. Then, an analytical HPLC system can start at the end of the control cycle. This means that the process outputs are delayed more than one cycle, so that the control cycle should be long enough to analyze samples and to complete numerical computation. In this work, the control unit can start computation for the next control cycle operation at

1 the beginning of current control cycle with up to previous cycle information. Therefore, the control
2 cycle can be shorten as long as the analysis time (including the sample preparation) if the control unit
3 can complete the computation within the analysis time (180 seconds).

5 ***4.3. Experimental validation***

6 For the experimental validation, the same system as the previous work [20] was chosen except
7 the type of packing material. The packing material has the same functional group but those are
8 chemically bonded (coated type was used in previous work). Therefore, the same isotherm models, bi-
9 Langmuir isotherms were chosen, and only the Henry's constants and NTPs were experimentally
10 measured. Therefore, it is the same as the proposed design campaign (Figure 1a). The tolerance value
11 for future prediction was set to 0.05 (larger than the first part of this work; to reduce computation time
12 for future prediction). This means that the tolerance limits are $\pm 0.2\%$ and $\pm 1.0\%$ for 99% and 95% of
13 set purities, respectively. Since the SMB system contains quite large system void volumes and the
14 NTPs were measured at low flow-rate (Table 1), the initial apparent dispersion coefficients, $D_{a,(R)}$ and
15 $D_{a,(S)}$ were arbitrary set to 1.5.

16 Figure 6 shows the experimental control histories for the standard operation with the fresh
17 feed mixture (14.1 g/L). The control unit successfully controlled the process to obtain 99% and 95%
18 purity products. At the beginning (up to 6th control cycle), the control unit predicted optimized future
19 operation with the initial guesses (the Henry's constants in Table 1 and the initial apparent dispersion
20 coefficients), so that the zone flow-rates were steeply changed at 7th cycle (the first control cycle with
21 parameter estimation). At the beginning, the flow-rate in the zone 1 was low and gradually increased,
22 so that the CST at desorbent port was contaminated with (R)-bicalutamide. Then, it took relatively
23 long cycle time to reach the set points for the raffinate purity and $R_{(R),Rcyl}$, cf. Eqs. (34) and (36).
24 Except the first optimization campaign (1 to 60 cycles), the controlled process outputs were converged
25 to the set-points in 20 control cycles, and the process inputs, four zone flow-rates were constantly
26 maintained. Note that the purity histories of the extract and raffinate at the sampling CSTs (dotted

1 lines) are obtained from online monitoring, and the purities at the extract and raffinate ports (solid
2 lines) are calculated from the estimated average concentrations. Because of a certain delay of online
3 monitoring for the product streams caused by the system void volumes, the measured purities (dotted
4 lines) followed the estimated purities (solid lines) with the same patterns. Since the column properties
5 varied quite a lot, the product streams were separately collected and analyzed for the last four control
6 cycles (in CSS) of each control campaign. Table 2 shows the set-points of subsequent optimization
7 campaigns, and the average process results in CSS of each optimization campaign. In CSS, separately
8 measured product purities are very close to the purity constraints. The liquid phase flow-rates in the
9 zones 3 and 4 ($Q_{L,3}$ and $Q_{L,4}$) are not much changed compared to the flow-rates in the zones 1 and 2
10 ($Q_{L,1}$ and $Q_{L,2}$) because the front ends of the internal profiles form stiff shock waves, cf. Figure 7b.
11 The set points of the first campaign (1 to 60 cycles) and the last campaign (181 to 220 cycles) were the
12 same, so that the control unit found the same optimized operating conditions as expected.

13 As discussed in the first part of this work, the estimated model parameters are not consistent
14 and not physically meaningful if the system and model do not match well. Figure 7a shows the
15 changes of estimated model parameters during the optimization campaigns of Figure 6. Up to the 6th
16 control cycle, the control unit used the linear isotherms (the initial guesses; all K values are zero but
17 $q_{Max}K$ values are not zero) with roughly chosen apparent dispersion coefficients, then the parameter
18 estimation started from the 7th control cycle. In 30 control cycles from the start-up, all model
19 parameters were converged and well maintained. Only the equilibrium constant for the achiral active
20 site, K_1 was dynamically changed in the last two optimization campaigns (140th to 220th cycles). It
21 seems that the chosen model cannot describe the system properly. However, the process outputs
22 implied unexpected fluctuation caused by experimental measurement error and non-identical column
23 properties described in Table 1. The retention contribution of the achiral sites, $q_{1,Max}K_1$ was relatively
24 small, and not much deviated. Therefore, the estimated retention behaviors in the first and last
25 optimization campaigns were not much different as shown in Figure 7b, especially the front and rear
26 profiles (black dashed circles) that were determined as an impurity in the product streams and the
27 recycle stream were well matched. The values of the objective function, G that represent the error of

1 parameter estimation was quite well maintained in low. In addition, table 3 shows the average
2 estimated model parameters and RSDs. Except the isotherm parameters for the achiral active sites
3 ($q_{1,Max}K_1$ and K_1), all model parameters were well maintained within 13% of RSD. As we discussed
4 in relation to Figure 1, a suitable process model should be specified before the on-line optimization is
5 activated and the model parameters are estimated. If the parameters estimated are consistent, this can
6 be seen as a strong indicator that the chosen model is appropriate to describe the process.

7 Further SMB experiments were done for three different operating modes with recovered feed
8 mixture (5.88 g/L of (R)-bicalutamide and 6.86 g/L of (S)-bicalutamide). Table 4 compares the
9 average operating conditions and performances in CSS. For all three operating modes, the complete
10 separation (99% of purities) was successfully accomplished. And the performance improved in two
11 advanced operating modes, the outlet stream swing (OSS) and the flow focusing (FF) were similar to
12 the simulation study (Figure 9 in [11]). Because of large void volume at the desorbent port,
13 contaminant remains quite long and consistently recycled to contaminate the products once the
14 desorbent port is contaminated. Therefore, the desorbent flow-rate in FF operating mode was not
15 decreased but maintained at the same level as the standard operation. However, the feed throughputs
16 were significantly increased both OSS and FF operating modes. Especially, the most promising FF
17 operating mode improved 46.0% of productivity and reduced 26.9% of desorbent consumption
18 compared to the standard operating mode.

19 During the experimental validation conducted in this work, 239 g of racemic mixture of
20 bicalutamides was separated. All extract and raffinate products were collected. After evaporating the
21 mobile phase, methanol, 88 g of (S)-bicalutamide and 87 g of (R)-bicalutamide were recovered with
22 97% of each purity. At the beginning of operation (start-up of process, effluents before reaching the
23 designated purity constraints) and after the operation (shut-down of process, residue solutes in the
24 columns), all effluents were collected together and 64 g of residue mixture was recovered.

26 ***4.4. Importance of considering system void volumes***

1 The on-line detectors in the extract and raffinate streams were connected directly after the
2 ports and the void volumes between the ports to the detectors were less than 6 ml, cf. Figure 2. Since it
3 was expected that the on-line detector signals can monitor the elution patterns of the product streams,
4 the profile reconstruction or foot-print observation could be applied. Figure 8 compared the UV
5 signals and the estimated concentration profiles right after the SMB ring in CSS of each optimization
6 campaign of Figure 6. For the extract stream, both of UV signals and estimated concentration profiles
7 described the dispersed profiles quite well. This means that the UV signals could be used for the
8 dynamic optimization using the above-mentioned profile reconstruction or the observation of foot-
9 prints. Due to the shock waves caused by the bi-Langmuir adsorption isotherms, the concentration
10 profiles in the raffinate stream form stiff changes as the estimated concentration profiles in Figure 8b.
11 However, the stiff patterns are quite dispersed in the UV signals even though the size of void volume
12 between the SMB ring and the detector is relatively small compared to the column size. To observe
13 more distinct stiff patterns using an UV detector, the flow-rate in the zone 4 should be lower. In this
14 case, the desorbent flow-rate should increase to maintain the same flow-rate in other zones, so that the
15 dynamic optimization using the UV signals may find sub-optimal operating conditions that consume
16 more desorbent.

17 Since the Mixer void volumes that represent the void volumes of the ports (the orange colored
18 region in Figure 2b) were fixed to the ports but do not travel with the column switching, so that it
19 causes critical remixing of the internal concentration profiles and unwanted product contamination. At
20 the end of the port switching interval, the feed port CST void volume contains high concentration of
21 the more-retained component, (R)-bicalutamide (at 2 of the axial distance in Figure 9a; impurity that
22 should not contaminate the raffinate stream), and the raffinate port CST void volume contains high
23 concentration of the less-retained component, (S)-bicalutamide (at 3 of the axial distance in Figure 9a;
24 impurity that should not contaminate the extract stream travelling through the desorbent port). On the
25 contrary, the Mixer void volumes of the extract and desorbent ports were relatively clean if the internal
26 concentration profiles were well posed. For the next cycle operation, the columns are shifted to the
27 next position. However, two CST void volumes at the feed and raffinate ports remain with the external
28 streams, and the raffinate and desorbent ports are contaminated with the high concentration

1 components contained in the feed and raffinate port void volumes, respectively. These unwanted
2 component propagation cause the humps developed in front of the shock fronts (A and B in Figure 9a).
3 To avoid extra contamination of the product streams caused by these humps, the flow-rates of the
4 zones 3 and 4 should be slower, so that it results more desorbent consumption and less feed
5 throughput.

6 To validate these humps experimentally, the developed internal concentration profiles were
7 eluted at the end of the SMB experiment and compared with the estimated internal concentration
8 profiles as shown in Figures 9b and 9c. Since the UV detector intensity is not linearly proportional to
9 the component concentrations in high concentration range and the developed internal concentration
10 profiles were additionally separated and dispersed during elution, both profiles were not perfectly
11 matched. However, some patterns are recognizable as indicated at the points A to E. The size of void
12 volumes at the feed and raffinate ports were relatively small (2 ml) compared to the column void
13 volume (52 ml). However, it caused critical contamination in high purity separation problems and a
14 falling-off in process performance.

15 In this work, the column positions were physically shifted, so that the void volumes of the
16 ports (supposed to be shifted with the columns) caused serious contamination in the well-posed
17 internal profiles. In other configurations, e.g. port-position shifting SMB unit, different sizes and
18 structures of the system void volumes may cause unwanted contamination that cannot be considered in
19 the corresponding ideal SMB. Consequently, as the results of this work can be concluded, it is
20 important to measure the size and structure of the system void volumes and to develop the
21 corresponding process model that can describe the behaviors of components in both columns and
22 system void volumes.

23

24 ***4.5. Computational aspects***

25 The control unit requires additional computation for the void volume models. The control unit
26 and the SMB interface program were executed on the same platform (a desk-top PC with intel® i7

1 CPU) for data exchange without latency. Therefore, the elapsed computation time for the control unit
2 may be longer than the results in the simulation study. To complete all relevant computation in one
3 control cycle, the tolerance value and the maximum iteration number for the optimizer were set to 0.05
4 and 100 respectively. Since the estimator conducted the parameter estimation with the fixed iteration
5 number (100) but without tolerance, the elapsed computation time for the parameter estimation was
6 around 60 seconds. As shown in Figure 10a, all computation was completed in one control cycle (180
7 seconds; one port switching interval). The average elapsed computation time for one cycle simulation,
8 \bar{t}_{Sim} was 28.1 ms with good R-square value (Figure 10b). This means that the total computation time
9 of the control unit can be reliably adjusted by the iteration number of a search method (the Nelder-
10 Mead method in this work) for future prediction and parameter estimation.

11

12 **5. Conclusion**

13 The proposed on-line optimization technique that exploits the equilibrium-dispersion model
14 for the separation columns and two additional void volume models, namely the Lag and the Mixer
15 models, could be successfully applied to optimize a pilot-scale four-zone SMB unit for the separation
16 of two bicalutamide enantiomers up to 99% of purity. Owing to an accurate description of the system
17 void volumes, the process outputs could be obtained without interruption of product streams.
18 Including an external HPLC unit for on-line monitoring, the SMB process was completely automated
19 using a tailored interface program that consistently communicates with the control unit. Thanks to the
20 accurate and fast numerical methods nowadays available, the proposed on-line optimization concept
21 has significant potential to be applied to solve other complex separation problems. The new SMB
22 design method proposed in the first part [11] and experimentally validated in this second part can
23 shorten the time needed to develop advanced separation processes and save resources. However, in
24 future work the proposed optimizer still needs to be complemented with robust control to allow for
25 disturbance rejections.

26

1 **Acknowledgement**

2 The authors cordially thank Dr. Martin Hedberg (Research Institute of Sweden, Södertälje,
3 Sweden) for the provision of bicalutamide racemates, Dr. Zoltan Horvath for the establishment of the
4 SMB monitoring system, and Mr. Jaeyoung Lee for the implementation of the SMB interface
5 program.

6

7 **References**

- 8 [1] D. B. Broughton, R. W. Neuzil, J. M. Pharis, C. S. Brearby, The parex process for recovering
9 paraxylene, *Chem. Eng. Prog.* 66 (1970) 70-75.
- 10 [2] H. Schramm, S. Grüner, A. Kienle, Optimal operation of simulated moving bed
11 chromatographic processes by means of simple feedback control, *J. Chromatogr. A* 1006 (2003)
12 3-13.
- 13 [3] S. Abel, G. Erdem, M. Mazzotti, M. Morari, M. Morbidelli, Optimizing control of simulated
14 moving beds – linear isotherm, *J. Chromatogr. A* 1033 (2004) 229-239.
- 15 [4] Y. Kawajiri, L. T. Biegler, Optimization strategies for simulated moving bed and powerfeed
16 processes, *AIChE J.* 52 (2006) 1343-1350.
- 17 [5] K. B. Lee, R. B. Kasat, G. B. Cox, N.-H. L. Wang, Simulated moving bed multiobjective
18 optimization using standing wave design and genetic algorithm, *AIChE J.* 54 (2008) 2852-
19 2871.
- 20 [6] A. Küpper, M. Diehl, J. P. Schlöder, H. G. Bock, S. Engell, Efficient moving horizon state and
21 parameter estimation for SMB processes, *J. Process Control* 19 (2009) 785-802.
- 22 [7] A. Toumi, S. Engell, Optimization-based control of a reactive simulated moving bed process for
23 glucose isomerization, *Chem. Eng. Sci.* 59 (2004) 3777-3792.

- 1 [8] E. Valery, C. Morey, Process and device for separating fractions of a mixture, US Patent
2 8,216,475 B2 (2012).
- 3 [9] C. Grossmann, C. Langel, M. Mazzotti, M. Morari, M. Morbidelli, Experimental
4 implementation of automatic ‘cycle to cycle’ control to a nonlinear chiral simulated moving bed
5 separation, *J. Chromatogr. A.* 1217 (2010) 2013-2012.
- 6 [10] P. Suvarov, A. V. Wouwer, J. W. Lee, A. Seidel-Morgenstern, A. Kienle, Control of incomplete
7 separation in simulated moving bed chromatographic process, *IFAC-PapersOnLine* 49 (2016)
8 153-158
- 9 [11] J. W. Lee, A. Kienle, A. Seidel-Morgenstern, On-line optimization of four-zone simulated
10 moving bed chromatography using an equilibrium-dispersion model: I. simulation study,
11 Submitted to *Chem. Eng. J.*
- 12 [12] J. W. Lee, A. Seidel-Morgenstern, Solving hyperbolic conservation laws with active
13 counteraction against numerical errors: Isothermal fixed-bed adsorption, *Chem. Eng. Sci.* 207
14 (2019) 1309-1330.
- 15 [13] C. Migliorini, M. Mazzotti, M. Morbidelli, Simulated moving-bed units with extra-column dead
16 volume, *AIChE J.* 45 (1999) 1411-1421.
- 17 [14] P. S. Gomes, M. Zabkova, M. Zabka, M. Minceva, A. E. Rodrigues, Separation of Chiral
18 Mixtures in Real SMB Units: The FlexSMB-LSRE®, *AIChE J.* 56(2010) 125-142.
- 19 [15] G. Hotier, R.M. Nicoud, Separation by simulated moving bed chromatography with dead
20 volume correction by desynchronization of periods, European Patent 688589 A1 (1995).
- 21 [16] J. Strube, K.-U. Klatt, G. Noeth, J. Greifenberg, S. Bocker, H. Kansy, P. Jahn, B. Justen,
22 Modular valve system for countercurrent chromatography process, US Patent 8,658,040 B2
23 (2014).

- 1 [17] K.-M. Kim, J. W. Lee, S. Kim, F. V. Santos da Silva, A. Seidel-Morgenstern, C.-H. Lee,
2 Advanced operating strategies to extend the applications of simulated moving bed
3 chromatography, *Chem. Eng. Technol.* 40 (2017) 2163-2178.
- 4 [18] P. S. Gomes, A. E. Rodrigues, Outlet streams swing (OSS) and multifeed operation of simulated
5 moving beds, *Sep. Sci. Technol.* 42 (2007) 223-252.
- 6 [19] S. Katsuo, M. Mazzotti, Intermittent simulated moving bed chromatography: 1. Design criteria
7 and cyclic steady-state, *J. Chromatogr. A* 1217 (2010) 1354-1361.
- 8 [20] H. Kaemmerer, Z. Horvath, J. W. Lee, M. Kaspereit, R. Arnell, M. Hedberg, B. Herschend, M.
9 J. Jones, K. Larson, H. Lorenz, and A. Seidel-Morgenstern, Separation of racemic bicalutamide
10 by an optimized combination of continuous chromatography and selective crystallization, *Org.*
11 *Process Res. Dev.* 16 (2012) 331-342.

12

1 **List of Tables**

- 2 Table 1 Properties of four columns used in the SMB unit and the Henry's constants, a_i and the
3 numbers of theoretical plates, NTP_i for the initial guesses.
- 4 Table 2 Applied set-points, purities and concentration ratios in the recycle stream, and the
5 corresponding average process results obtained in cyclic steady-state (CSS) of the on-line
6 optimization experiment described in Figure 6.
- 7 Table 3 Average and RSD of the estimated adsorption isotherm parameters and apparent
8 dispersion coefficients obtained from 30th to 220th control cycles of the on-line
9 optimization experiment described in Figure 7.
- 10 Table 4 Operating conditions optimized by the on-line optimization and average process results in
11 cyclic steady-state (CSS) for the standard and two advanced (OSS and FF) operating
12 modes.

13

14 **List of Figures**

- 15 Figure 1. (a) Proposed design steps with on-line optimization.
16 (b) Schematic flow-diagram of the proposed on-line optimization [11]. Op. Cond.:
17 operating conditions, four zone flow-rates
- 18 Figure 2. Schematic illustration of the SMB process including various system void volumes (a) and
19 Size and structure of considered void volumes at four ports (b).
20 Ports are fixed, but the position of the columns are switched.
21 Orange regions: system void volumes inside of the SMB ring, but not switched.
- 22 Figure 3. (a) Schematic illustration of SMB product stream profiles at the extract port in the SMB
23 ring (lower), at the small sampling CST (middle), and at the large sampling CST (upper).
24 Marked by A is the representative sampling time.

1 (b) Schematic flow-diagrams of the full sampling (used in this work) and the by-pass
2 sampling CSTs.

3 Figure 4. Schematic illustration of hierarchical communication structure between the control unit
4 and SMB process.

5 RS-232: serial communication protocol between the control PC and devices;
6 Platform I/O: standard input/output protocol of the control PC platform (Windows® 7)

7 Figure 5. Representative chromatogram of the analytical HPLC system (Column: ChiralPak IA,
8 3 μ m, 0.46 \times 15 cm; Mobile phase: methanol, 40 °C; Detection: UV, 300 nm).

9 Acquisition of analytical HPLC chromatogram is started 20 seconds after the beginning
10 of the corresponding control cycle. The sample collection offsets of the extract, recycle,
11 and raffinate streams are 0.067 (12 seconds; A), 0.289 (52 seconds; B), and 0.511 (92
12 seconds; C), respectively.

13 Figure 6. On-line optimization histories of the process inputs (Q_L) and the controlled variables,
14 purities and R_{Rcyl} in Eqs. (34 - 37).

15 Set-points and results in cyclic steady-state are in Table 2.

16 Figure 7. (a) On-line estimator histories in terms of the process model parameters in Eq. (1) and the
17 estimation error, G in Eq. (32) during the experiment described in Figure 6 (average
18 values and RSDs in Table 3).

19 (b) Comparisons of estimated internal concentration profiles at 60th and 220th cycles.

20 Figure 8. Comparisons of the normalized extract (a) and raffinate (b) elution patterns of the on-line
21 UV signals (process) and the estimated concentration profiles (control unit) obtained from
22 the experiment described in Figure 6.

23 Figure 9. (a) Estimated internal concentration profiles at the end of experiment. A and B indicate
24 contaminations caused by the raffinate and feed port void volumes, respectively.

25 (b) Superposed internal concentration profiles of Figure 9a. Characteristic profile patterns
26 are marked by A to E for comparisons.

1 (c) UV profiles detected at the outlet of the zone 4 during internal profile elution after the
2 experiment. Characteristic profile patterns are marked by A to E for comparisons.

3 Figure 10. (a) Histories of elapsed computation time of the control unit.

4 (b) Elapsed computation time in terms of the number of simulation.

5 \bar{t}_{sim} : average elapsed time for one port switching internal simulation in the control unit

6

Table 1.

	Column 1	Column 2	Column 3	Column 4	Average / RSD [%]
Adsorbent [g]	45.03	45.01	45.03	45.06	45.03 / 0.02
Length [cm]	14.75	14.67	14.72	14.64	14.67 / 0.38
ε [-]	0.789	0.782	0.787	0.772	0.783 / 1.02
$a_{(R)}^{1)}$ [-]	2.594	2.684	2.810	2.745	2.708 / 3.40
$a_{(S)}^{1)}$ [-]	0.319	0.349	0.364	0.339	0.343 / 5.54
$NTP_{(R)}^{1)}$ [-]	298	582	523	342	436 / 31.55
$NTP_{(S)}^{1)}$ [-]	531	1317	1135	628	903 / 42.38

¹⁾ Measured at 3.0 ml/min

Table 2.

		Cycles	1 – 60	61 – 100	101 – 140	141 – 180	181 – 220
Set-Points , Eq. (33)	\widehat{Pu}_{Extr} [%]		99	95	95	99	99
	\widehat{Pu}_{Raff} [%]		99	95	95	99	99
	$\widehat{R}_{(R),Rcyl}$		0.50	0.50	0.10	0.10	0.50
	$\widehat{R}_{(S),Rcyl}$		0.10	0.10	0.02	0.02	0.10
		CSS Cycles	57 – 60	97 – 100	137 – 140	177 – 180	217 – 220
Results ¹⁾	Pu_{Extr} [%] ²⁾		98.9	94.7	94.5	98.9	98.9
	Pu_{Raff} [%] ²⁾		99.1	94.9	94.9	99.1	98.8
	Productivity [g/L/h]		5.75	7.31	7.45	5.20	5.74
	D.C. [L/g]		0.70	0.44	0.58	1.01	0.72
	$Q_{L,Z1}$ [ml/min]		32.70	28.83	32.63	36.80	33.08
	$Q_{L,Z2}$ [ml/min]		22.30	21.10	21.25	22.43	22.33
	$Q_{L,Z3}$ [ml/min]		25.45	25.10	25.58	25.70	25.50
	$Q_{L,Z4}$ [ml/min]		20.10	20.40	20.08	19.75	20.08

¹⁾ Average values for last four control cycles (cyclic steady-state)

²⁾ From the analysis of product effluent separately collected for last four control cycles (cyclic steady-state)

Table 3.

Parameters, Eqs. (1) and (2)	Average	RSD [%]
$D_{a,(R)}$ [cm ² /min]	0.69	12.9
$D_{a,(S)}$ [cm ² /min]	0.63	10.2
$q_{1,Max}K_1$ [-]	0.62	22.5
$q_{2,Max}K_{2,(R)}$ [-]	1.83	5.6
$q_{2,Max}K_{2,(S)}$ [-]	0.2	10.8
K_1 [L/g]	0.162	53.5
$K_{2,(R)}$ [L/g]	0.110	11.1
$K_{2,(S)}$ [L/g]	0.012	7.6

Table 4.

Operating Mode	Standard	OSS, $F_{Op} = 0.5$	FF, $F_{Op} = 0.5$
$Q_{L,Z1}$ [ml/min]	32.60	33.53	32.59
$Q_{L,Z2}$ [ml/min]	23.13	22.55	22.01
$Q_{L,Z3}$ [ml/min]	25.83	25.98	25.70
$Q_{L,Z4}$ [ml/min]	20.50	20.93	20.48
$Q_{L,Feed}$ [ml/min]	2.70	3.43	3.69
$Q_{L,DSrb}$ [ml/min]	12.10	12.60	12.10
Pu_{Extr} [%]	99.1	99.3	99.0
Pu_{Raff} [%]	99.0	99.2	99.0
Productivity [g/L/h], Eq. (38)	4.21	5.31 (26.1%) ¹⁾	6.15 (46.0%) ¹⁾
D.C. [L/g], Eq. (39)	0.90	0.78 (14.1%) ²⁾	0.66 (26.9%) ²⁾

¹⁾ Improvement of productivity compared to the standard operation

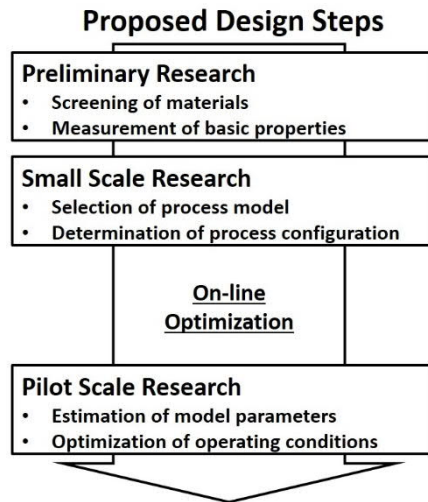
$$= 100 \left(\frac{\{\text{Productivity in Advanced Operation}\}}{\{\text{Productivity in Standard Operation}\}} - 1 \right)$$

²⁾ Improvement of desorbent consumption compared to the standard operation

$$= 100 \left(1 - \frac{\{\text{D.C. in Advanced Operation}\}}{\{\text{D.C. in Standard Operation}\}} \right)$$

Figure 1.

a)



b)

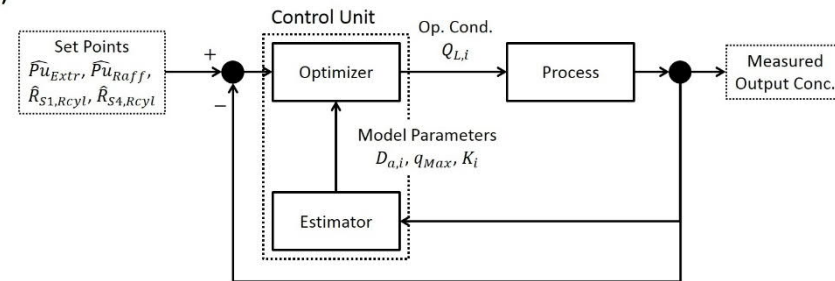


Figure 3.

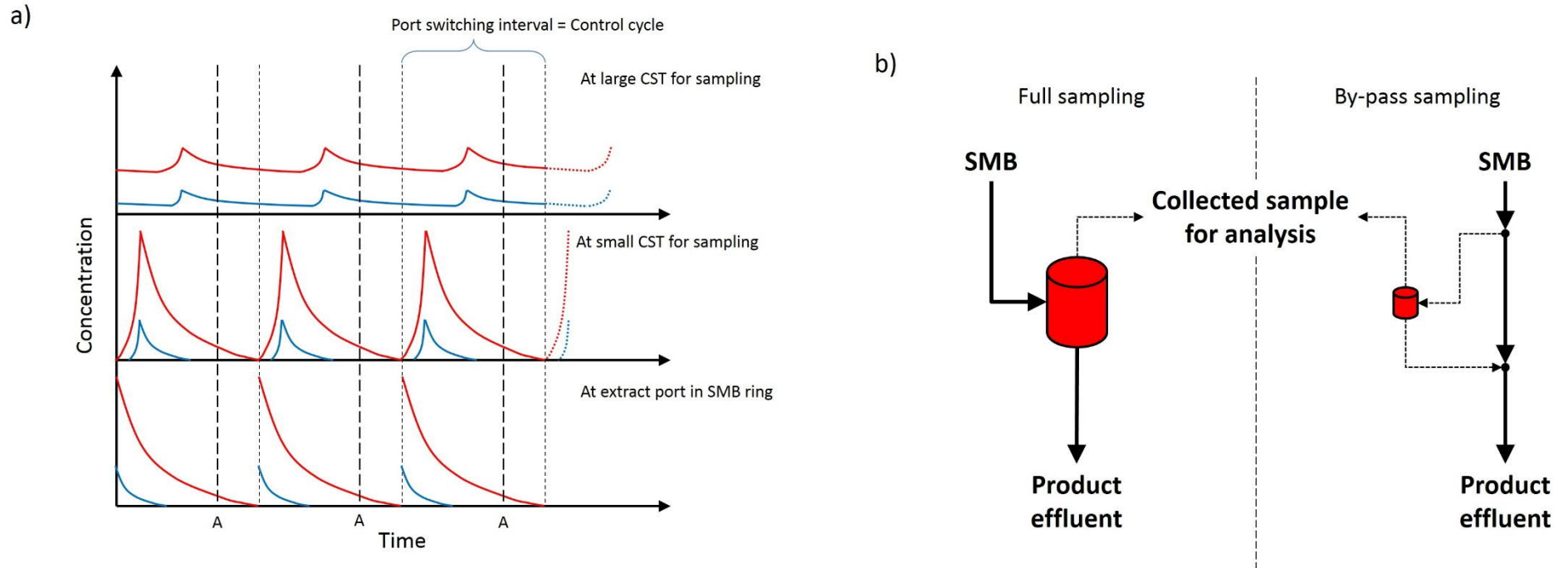


Figure 4.

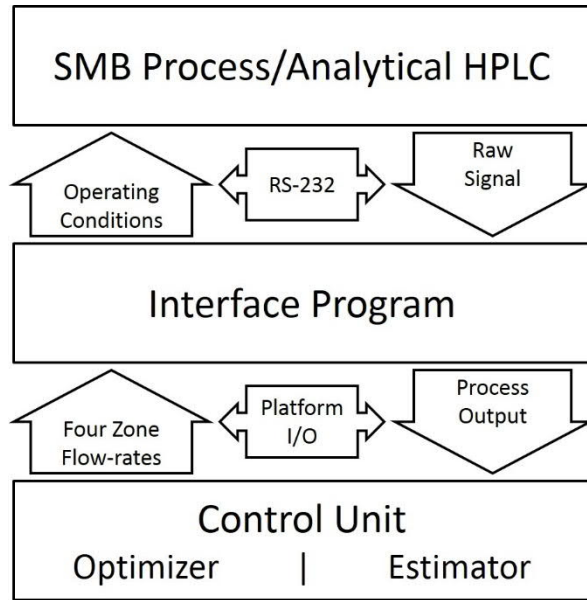


Figure 5.

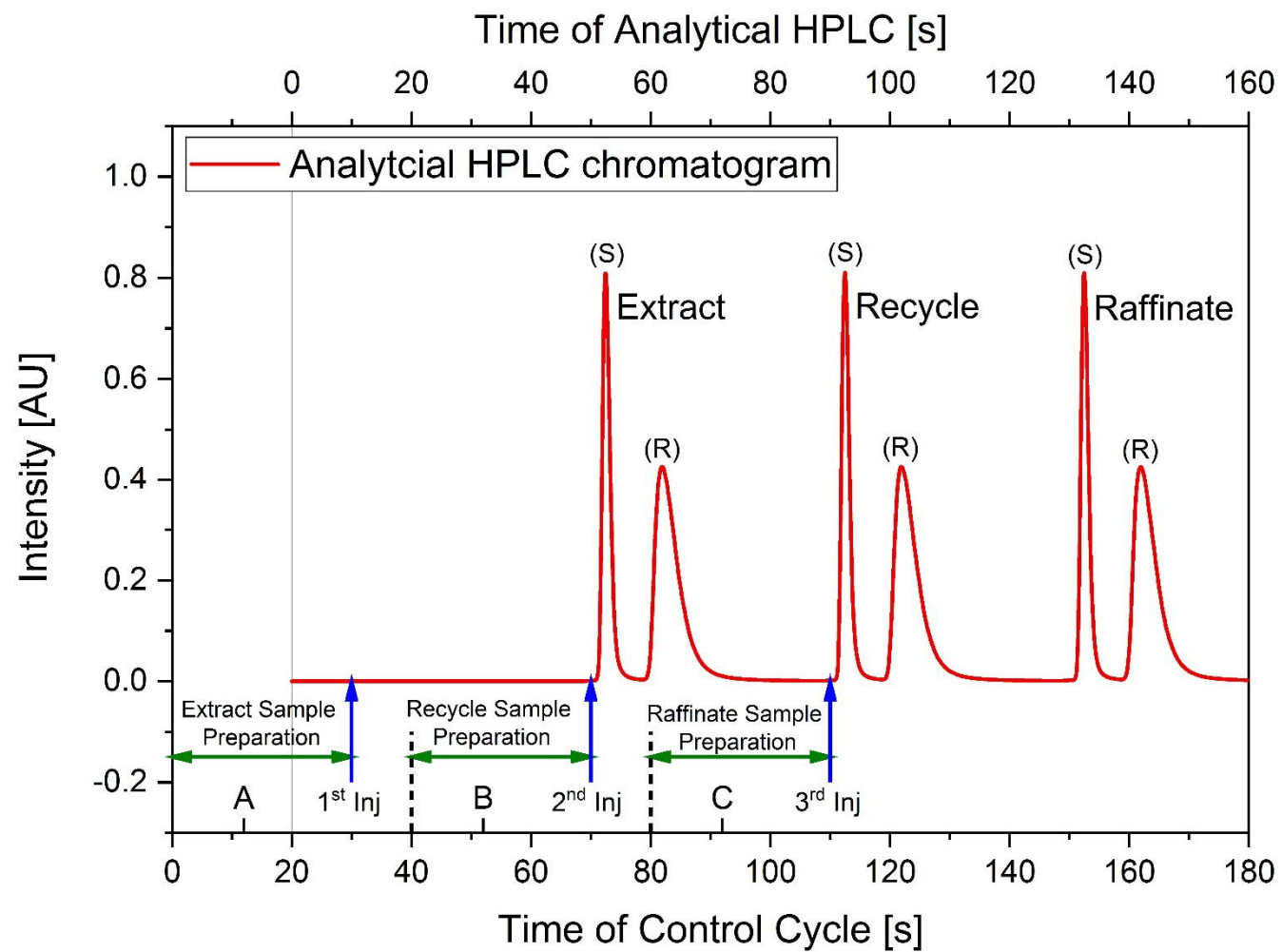


Figure 6.

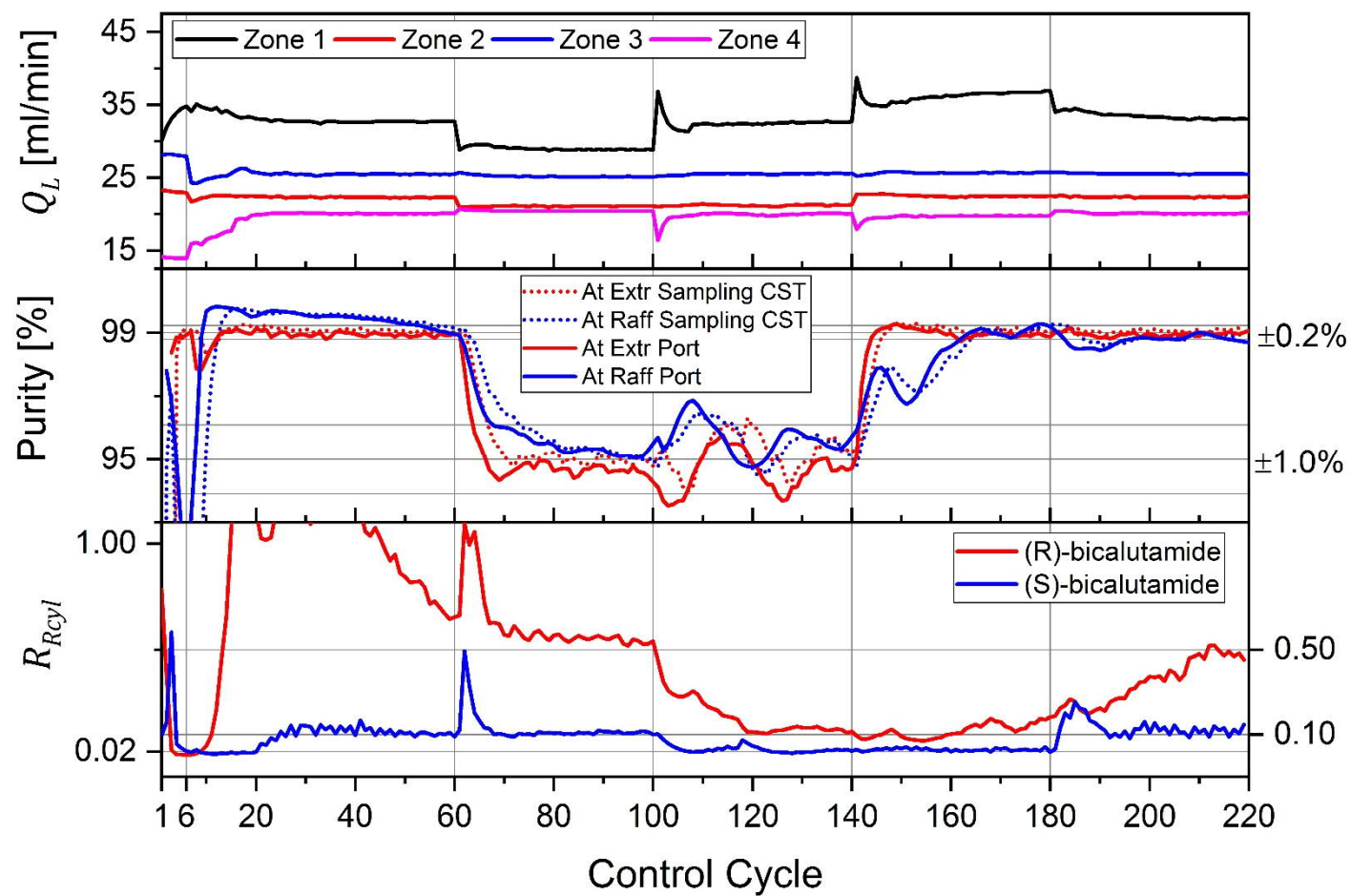


Figure 7.

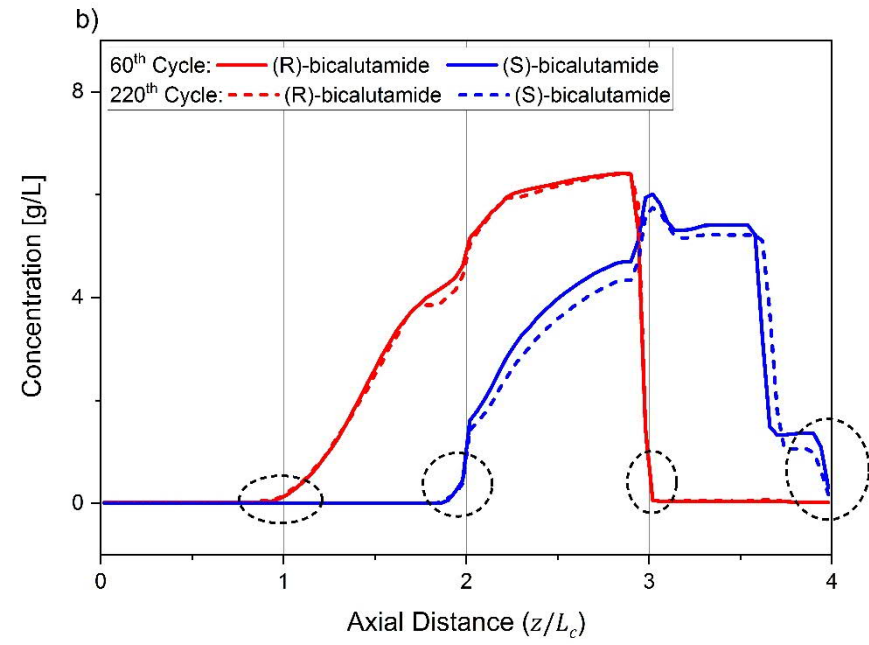
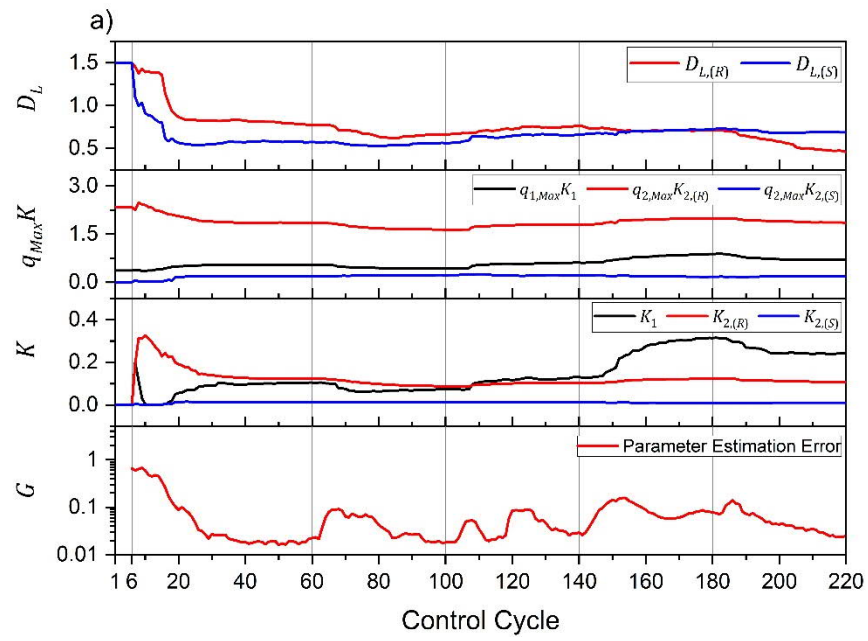


Figure 8.

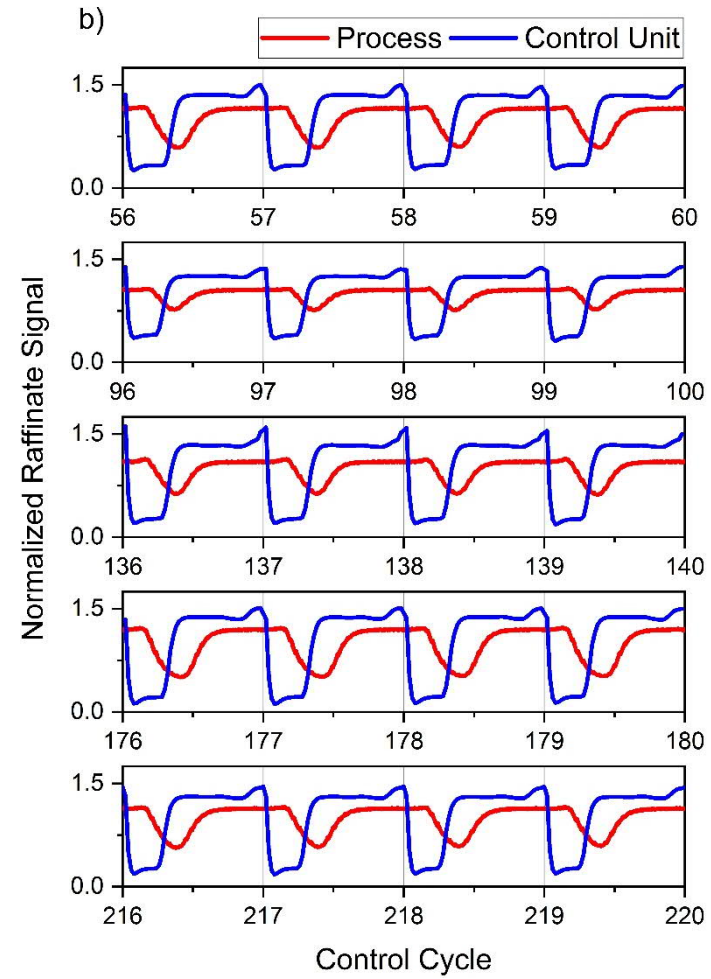
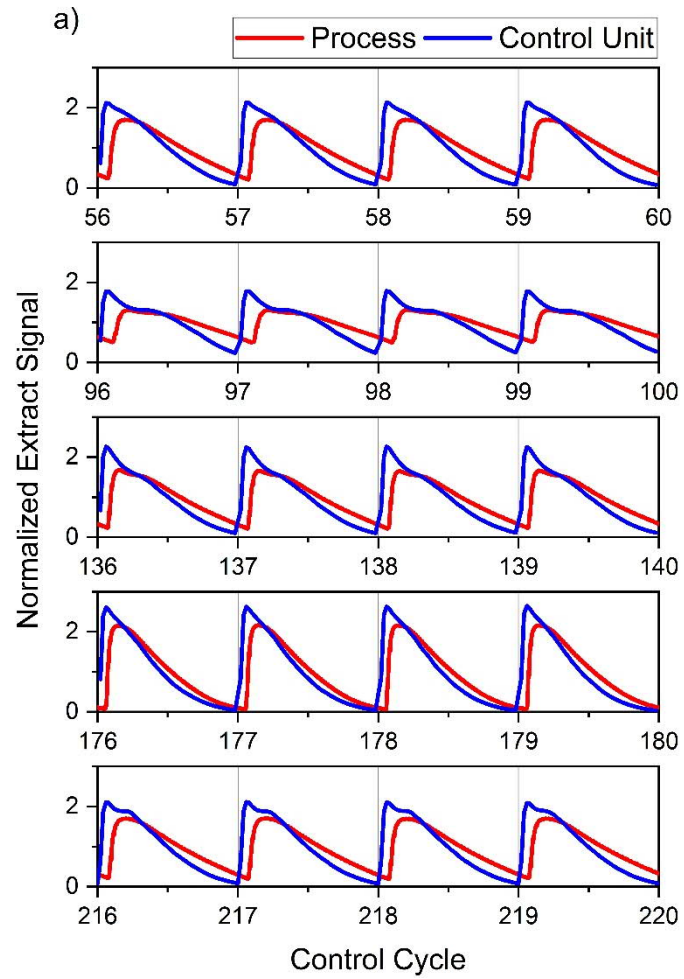


Figure 10.

